Engineering Structures 123 (2016) 77–88

Contents lists available at ScienceDirect

Engineering Structures

journal homepage: www.elsevier.com/locate/engstruct

Behavior of hollow FRP–concrete–steel columns under static cyclic axial compressive loading

Omar I. Abdelkarim, Mohamed A. ElGawady *

Dept. of Civil, Architectural, and Environmental Engineering, Missouri University of Science and Technology, USA

ARTICLE INFO

Article history:
Received 3 January 2016
Revised 10 April 2016
Accepted 17 May 2016
Available online 10 June 2016

Keywords:
Bridge columns
Precast columns
Composite columns
Hollow columns
Axial loading

ABSTRACT

This paper presents the behavior of hollow fiber reinforced polymer–concrete–steel (HC-FCS) columns under axial compressive loading. The typical HC-FCS column consists of a concrete shell sandwiched between an outer fiber reinforced polymer (FRP) tube and an inner steel tube. The inner steel and outer FRP tubes provide continuous confinement for the concrete shell; hence, the concrete shell achieves a significantly higher strain, strength, and ductility compared to the unconfined concrete in conventional columns. The HC-FCS column represents a compact engineering system; the steel and FRP tubes act together as stay-in-place formworks. The effect of the fiber orientation and the steel tube diameter-to-thickness ratio (D_i/t_s) on the compressive behavior of HC-FCS columns was investigated. Ten HC-FCS cylinders with different steel tube D_i/t_s ratios and three concrete-filled fiber tubes (CFFTs) were manufactured and tested under static cyclic axial compressive loading in addition to three empty steel tubes. The behavior of the HC-FCS columns was complicated and related mainly to the stiffness of the FRP and steel tubes, which controlled the direction of the concrete dilation under axial load. HC-FCS columns with FRP tubes made with fibers oriented at ±45° showed low axial compressive strengths and high ultimate strains. HC-FCS columns with wet lay-up FRP tubes that had ±45° and 0° (hybrid FRP) exhibited high axial strengths and strains. The failure of the HC-FCS columns with hybrid FRP tubes consisted of two stages. The first stage was the rupture of the unidirectional FRP tube (outer tube), and the second stage was the reorientation of the oriented FRP tube exhibiting high axial strains.

1. Introduction

Hollow concrete columns have been introduced to reduce the mass of the solid columns and, hence, reduce the internal forces under seismic loading especially when the bridge located in the high seismic regions. As a result, the hollow columns reduces the base shear and moment on the foundation. Therefore, the required foundation dimensions are also reduced substantially, thereby lowering the construction time and costs. In the last few decades, concrete-filled tubular columns have been employed widely in the U.S., Japan, China, and Europe. Concrete-filled tubular columns have many benefits, including a light weight-to-strength ratio, concrete confinement, and short construction time. The seismic behavior of the concrete-filled tubular columns has been extensively studied under different loadings [e.g., 1–6].

Double-skin tubular columns have been developed as a new version of the concrete-filled tubular columns [7]. A double-skin tubular column consists of a concrete shell that is sandwiched between two generally concentric steel tubes with a hollow inner tube. Therefore, such columns combine the benefits of concrete-filled tubular columns with the benefits of hollow concrete columns. They have been extensively studied [8,9]. More recently, Teng et al. [10] used fiber reinforced polymer (FRP) as an outer tube and the steel as an inner tube in the double-skin tubular columns. This system combines and optimizes the benefits of all three materials: FRP, concrete, and steel in addition to the benefits of the hollow concrete columns to introduce hollow FRP–concrete–steel columns (HC-FCS). The HC-FCS columns have been investigated extensively under axial compression loading [11–16]. The results of the axial compression experiments showed high concrete confinement and ductility.

Most of the studies conducted on the confinement of concrete using FRP used unidirectional fibers oriented in the hoop direction. Very few researchers used angular fibers instead of the unidirectional fibers in the concrete-filled fiber tubular and reinforced concrete columns [17–21]. According to the writers' best knowledge, no previous studies have been done investigating HC-FCS columns with angular fibers under axial compressive loading. The studies

* Corresponding author.
E-mail addresses: oiafgc@mst.edu (O.I. Abdelkarim), elgawadym@mst.edu (M.A. ElGawady).

http://dx.doi.org/10.1016/j.engstruct.2016.05.031
0141-0296/

Table 1
Description of the tested specimens.

Group no.	Specimen number	Outer FRP tube	Inner steel tube D_i (t_s) (mm)	Concrete shell thickness (mm)
A	HC-CIII45-25-64	CFRP – Three layers 45°	101.6 (1.6)	54
	HC-CIII45-32-38		76.2 (2.0)	67
	HC-CIII45-38-32		50.8 (1.6)	80
	CFFT-CIII45		–	–
B	HC-GIII45-25-64	GFRP – Three layers 45°	101.6 (1.6)	54
	HC-GIII45-32-38		76.2 (2.0)	67
	HC-GIII45-38-32		50.8 (1.6)	80
	CFFT-GIII45		–	–
C	HC-GII45/I0-25-64	GFRP – Two layers 45° + One Layer 0°	101.6 (1.6)	54
	HC-GII45/I0-32-38		76.2 (2.0)	67
	HC-GII45/I0-38-32		50.8 (1.6)	80
	CFFT-GII45/I0		–	–
D	HC-GI45/II0-25-64	GFRP- One layer 45° + Two Layers 0°	101.6 (1.6)	54
E	Steel tube A	–	101.6 (1.6)	–
	Steel tube B	–	76.2 (2.0)	–
	Steel tube C	–	50.8 (1.6)	–

revealed that the angular fibers had a gradual failure instead of the sudden rupture of the unidirectional fibers. Au and Buyukozturk [21] studied the stacking sequence of the hybrid system using the unidirectional angular fibers in concrete-filled fiber tubular columns under axial loading. This study revealed that using the unidirectional angular fibers improves the strength and ductility of the confined concrete. The unidirectional fibers on the outer surface provided the majority of the confinement. Hence, they ruptured first. Then, the angular fibers continued to contain the concrete shell until high ductility was reached.

In an HC-FCS system, the concrete shell between the outer FRP tube and the inner steel tube is usually thin. Self-consolidating concrete (SCC) represents a good option for preventing honeycomb and lessening the problem of consolidating and vibrating concrete. SCC has a high flowability and a moderate viscosity, giving it the ability to self-consolidate. A balance between dosages of superplasticizers or high range water reducers (HRWR) must be achieved to increase the flowability and dosages of viscosity modifying agents (VMA) to enhance stability and reduce segregation.

2. Research significance

This paper presents the behavior of the HC-FCS columns under cyclic axial compressive loading. The HC-FCS column has several benefits such as its use of 60–75% less concrete material than the solid cross-sectional column and both steel and FRP tubes acting as stay-in-place formworks. The corrosion-free FRP outer tube and concrete shell provide the inner steel tube with high corrosion resistance. However, the inner steel tube may require additional corrosion protection in the inner side using an anti-corrosion agent. The FRP and steel tubes reduce concrete shell shrinkage as they do not allow significant water evaporation. The investigated HC-FCS columns had new features different from those investigated in the literature. The previous studies were conducted on HC-FCS columns using unidirectional FRP tubes oriented in hoop direction and steel tubes with a low diameter-to-thickness ratio that ranged from 11.9 to 32 and with concrete shell thickness is about 35% of the column's diameter. However, the investigated HC-FCS columns in this paper were constructed using a thin to thick concrete shell thickness (25–38% of the column's diameter), relatively high diameter-to-thickness ratios of the steel tube (D_i/t_s = 32–64), low to high FRP confinement stiffness, the fiber in the FRP is oriented at ±45° and hybrid FRP system.

3. Experimental program

3.1. Test specimens

A total of 16 specimens were tested under cyclic axial compressive loading. Table 1 summarizes the specimens' details and variables. The test matrix included 10 HC-FCS, 3 CFFT, and 3 bare steel tube specimens. All of the CFFT and HC-FCS specimens were identical and had an outer diameter of 210 mm and a height of 406 mm (Fig. 1). The thirteen specimens were sorted into four groups. The nomenclature of the test specimens used in the current study consisted of four syllabi. The first syllabus referred to the type of the specimen where "HC" referred to the HC-FCS cylinders and "CFFT" referred to concrete-filled fiber tubes. The second syllabus referred to the type of FRP where "C" was for carbon and "G" was for glass; this was followed by the number of layers in *Latin* letters and the direction of fibers measured from the hoop direction (45° or 0° or a combination). In the case of the combination of angle-plied FRP and the unidirectional FRP, the unidirectional FRP was always in the outer surface. The third syllabus referred to the percent of the concrete shell thickness relative to the outer diameter. The fourth syllabus referred to the outer diameter-to-thickness (D_i/t_s) ratio of the steel tube. The third and fourth syllabi do not exist in the case of the CFFTs.

For instance, Group A consisted of three HC-FCS cylinders and one CFFT cylinder. The outer tubes of this group were made of three layers of ±45° *carbon* fiber reinforced polymer (CFRP), while the inner steel tubes of the HC-FCS cylinders had diameters of 101.6 mm, 76.2 mm, and 50.8 mm with steel diameter-to-thickness (D_i/t_s) ratios of 64, 38, and 32, respectively.

3.2. Material properties

Table 2 shows the mix design of the SCC that was used. The average cylindrical concrete compressive strength (f'_c) at 28 days was 55 MPa.

According to ASTM D3039 [22], longitudinal and radial coupons with widths of 25 mm were cut from one-layer Glass and Carbon FRP tubes. One horizontal and one vertical strain gauge were attached to the mid height of the longitudinal FRP coupon. Two strain gauges were attached to the middle of the radial disk. Under tensile tests with a displacement loading rate of 1.27 mm/min., all of the FRP coupons and radial samples failed by debonding

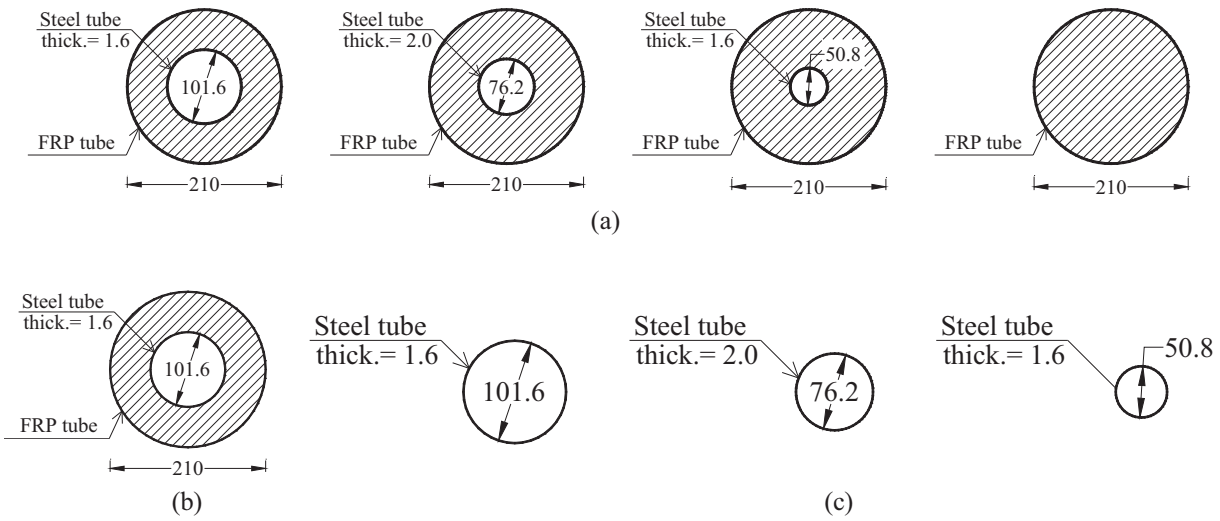

Fig. 1. Typical cross-sections of the test specimens in groups: (a) Groups A/B/C, (b) Group D, and (c) Group E.

Table 2
SCC mixture proportions.

w/cm	Cement (kg/m^3)	Fly ash (kg/m^3)	Water (kg/m^3)	Fine aggregate (kg/m^3)	Coarse aggregate (kg/m^3)	HRWRA (kg/m^3)	VEA (kg/m^3)
0.38	350	174	198	830	830	2.1	0.7

Table 3
Properties of saturated FRP according to manufacturer's data.

Material	Nominal thickness/layer (mm)	Young's modulus, *E* (GPa)	Tensile strength (MPa)	Ultimate strain (%)
CFRP-45°	0.86	47.9	661	1.40
GFRP-45°	0.86	18.6	279	1.50
GFRP-0°	1.30	26.1	575	2.20

between the two 45° plies [±45°] without fiber rupture with ultimate tensile stress for the specimens of about 73.0 MPa. This low stress value occurred as the provided FRP fabric were manufactured using neither woven nor filament techniques with a fiber orientation at ±45°. Also, testing coupons having small width of only 25 mm which did not allow fiber continuity led to this reported small stress values. The properties of the saturated FRP as provided by the manufacturer data sheet are summarized in Table 3.

Standard coupons were cut longitudinally from a steel tube for tensile tests according to ASTM A1067 [23]. The steel coupon tests were conducted under a displacement control of 0.76 mm/min. A strain gauge was attached to the mid height of the steel coupons (Fig. 2a). All steel coupons failed by yielding in the neck (Fig. 2b). The results showed that the yield stress, tensile stress, the Young's modulus, and the ultimate strain of the steel tubes were 620 MPa, 620 MPa, 200 GPa, and 0.4%, respectively.

Three hollow steel tubes similar to those used in the HC-FCS cylinders were tested under monotonic axial compression. Strain gauges were mounted, two in the hoop direction and two vertical on the outer surfaces of the steel tubes, as shown in Fig. 3. Steel Tube A, of a diameter of 101.6 mm, and Tube B, with a diameter of 76.2 mm, failed at ultimate axial loads of 302 kN and 296 kN, respectively, by local buckling in the elephant's foot mode as shown in Fig. 4a and b, respectively. This corresponded to maximum stresses of 592 MPa and 617 MPa, respectively (Fig. 5). However, Steel Tube C failed by global buckling and local buckling in the elephant's foot mode, as shown in Fig. 4c, at a load of 83 kN

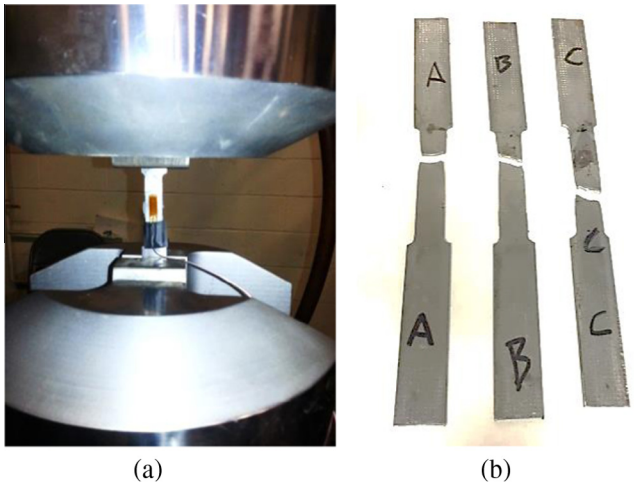

Fig. 2. Steel coupon tests: (a) testing of steel coupon and (b) rupture of steel coupons.

corresponding to a stress of 315 MPa (Fig. 5). The failure load of Tube C was significantly lower than the other tubes because the global buckling occurred early. In general, the behavior of the steel tubes was similar, starting with linear behavior until the axial compressive strain ranged from 0.4% to 0.5%. After that, the stress

Fig. 3. Testing of steel tube under compressive loading.

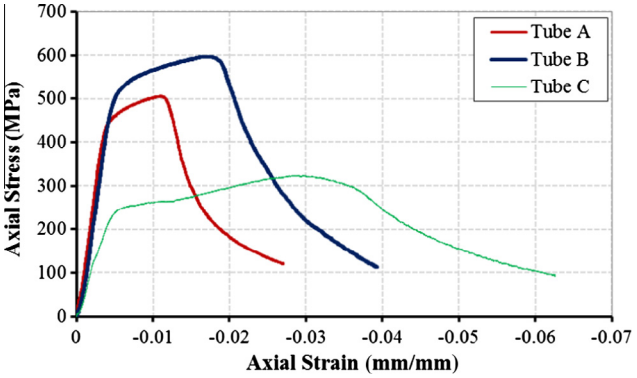

Fig. 5. Axial strain–stress relation of the steel tubes.

hardened with a lower stiffness until the maximum axial stress was reached. Each steel tube then suffered stress softening due to the local or global buckling until the end of the test.

3.3. Instrumentation and test setup

Compression tests were carried out using an MTS machine with a loading rate of 0.5 mm/min. All test data, including the strains, loads, and displacements, were recorded using a data acquisition system. Two horizontal and two vertical strain gauges were installed on the outer surface at the mid-height of the FRP tube. Likewise, two horizontal and two vertical strain gauges were installed on the outer surface at the mid-height of the steel tube. In addition, two string potentiometers were attached on the outer surface of the FRP tube to obtain the axial deformation of the middle region of 140 mm for each specimen. Fig. 6 illustrates the test setup of the investigated cylinders.

Fig. 6. Test setup of the investigated specimens.

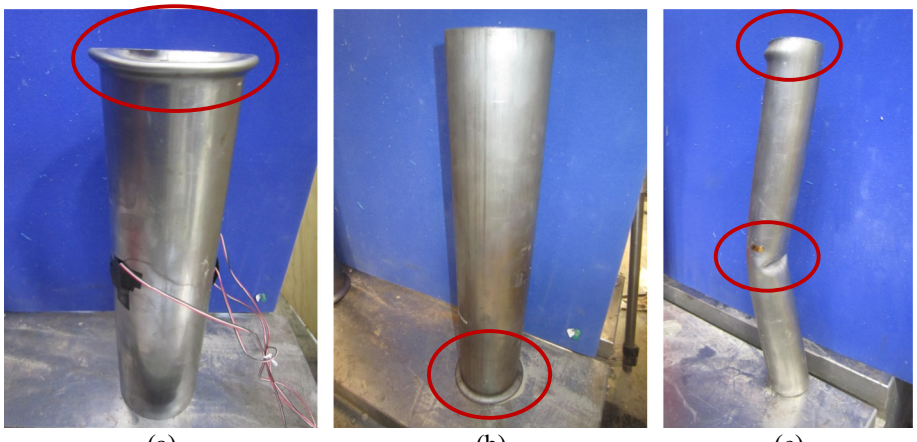

Fig. 4. Modes of failure of the steel tubes: (a) elephant foot of tube A, (b) elephant foot of tube B, and (c) global buckling and elephant foot of tube C. Note: circles were drawn around the local or global buckling.

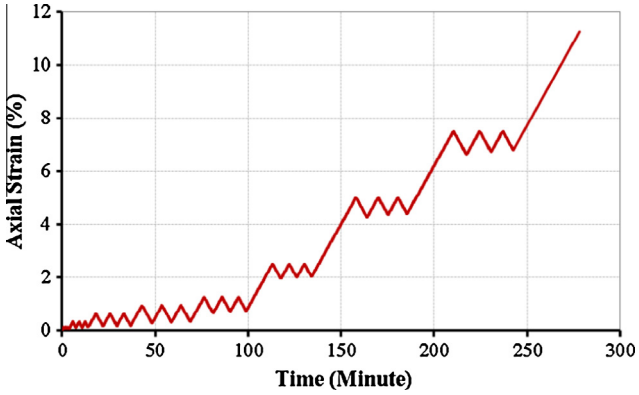

Fig. 7. Cyclic loading scheme.

3.4. Loading protocol

All specimens were tested under compression loading on a cyclic scheme, as shown in Fig. 7. The cyclic compression involved full loading/unloading cycles, where the unloading of each cycle was designed to terminate at 0.4 kN (near zero), and the reloading of each cycle was designed to terminate at the unloading displacement of the same cycle. The loading scheme followed nine steps, beginning at an axial strain of 0.125%. The axial strain was increased gradually until specimen failure or maximum displacement of the machine, which corresponded to an overall strain of the cylinder of 11.25%. Each loading step was repeated for three cycles.

4. Results and discussions

4.1. General behavior

Fig. 8 illustrates the axial strain versus axial load hysteretic curves for the groups' specimens. The axial compressive strains were obtained from the average readings of the two string potentiometers and were represented using negative values. The behaviors of the specimens in each group were similar and hence the behavior of one specimen out of each group will be given in the next section.

4.1.1. Group A (three layers of ±45°CFRP)

For the specimen HC-CIII45-25-64, the load increased approximately linear until reaching the peak axial load of 1356 kN at an axial strain of approximately 0.14% (Fig. 8a). The load softened with the strain increasing directly after the peak axial load without strain hardening (unlike concrete cylinders confined using 0/90° FRP). This behavior occurred because of the reorientation of the ±45° fiber. The axial load dropped by 41% to 800 kN at an axial strain of 0.02. The load was approximately constant until an axial strain value of 0.13, when the loading machine reached its maximum stroke without rupture of the FRP tube (Fig. 9). The post-test visual inspection revealed that the steel tube displayed severe local buckling (Fig. 9) which contributed to the softening of the axial load.

4.1.2. Group B (three layers of ±45° GFRP)

For the specimen HC-GIII45-25-64, the load increased approximately linear until a peak axial load of 1522 kN corresponding to an axial strain of approximately 0.80% (Fig. 8b). Beyond that the

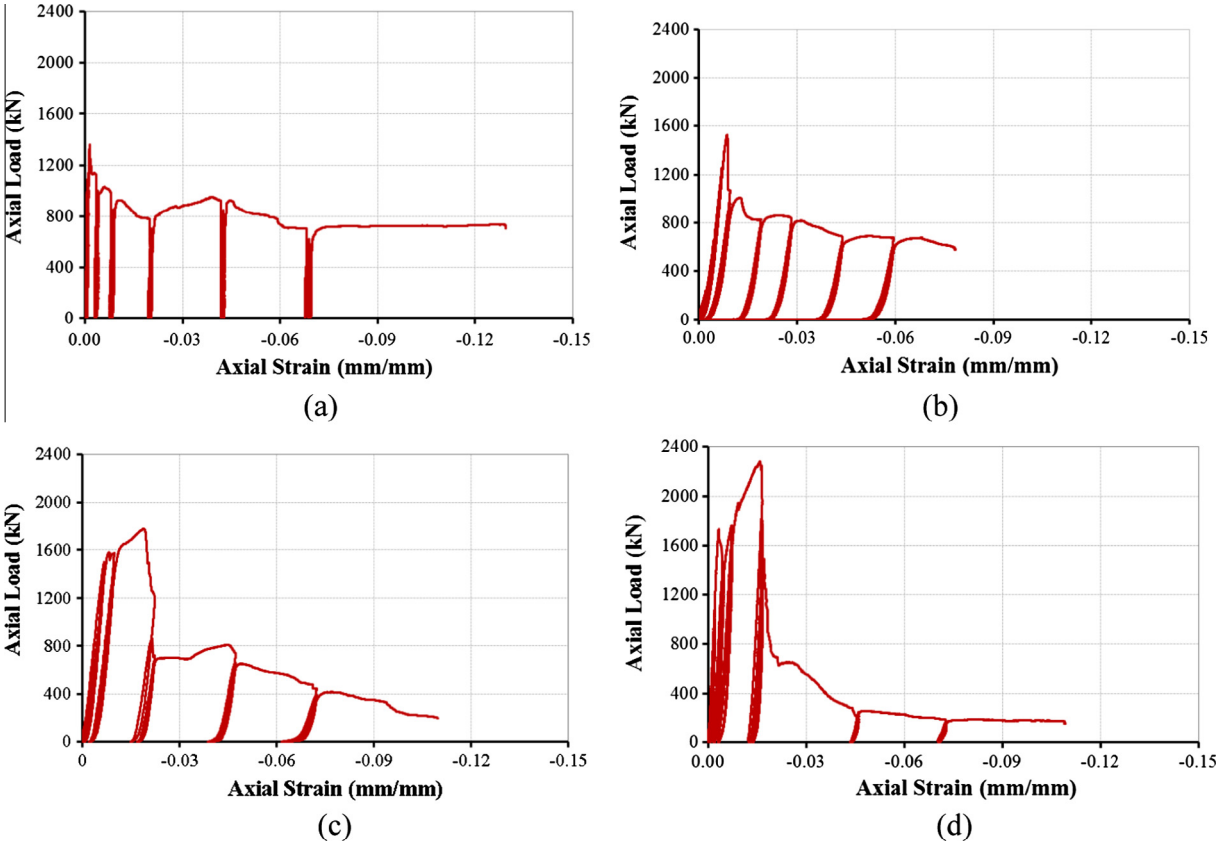

Fig. 8. Axial strain–axial load relation of the cylinders: (a) HC-CIII45-25-64, (b) HC-GIII45-25-64, (c) HC-GII45/I0-25-64, and (d) HC-GI45/II0-25-64.

Fig. 9. Modes of failure of all of the specimens and their steel tube local buckling.

specimen displayed strength softening without any hardening which was similar to the behaviors of the specimens in Group A. The axial load dropped to 635 kN with a loss of approximately 58% at an axial strain of 0.044. After that, the axial load kept constant until an axial strain of 0.08. The test was terminated at a vertical displacement of 33.0 mm without rupture of the GFRP tube (Fig. 9). The steel tube buckled locally, as observed in the other specimens.

4.1.3. Group C (two layers of ±45° GFRP/one layer of unidirectional GFRP)

For the specimen HC-GII45/I0-25-64, the load increased approximately linear until an axial load of 1546 kN corresponding to an axial strain of approximately 0.76% (Fig. 8c). Beyond that, the specimen displayed load hardening until a peak axial load of 1770 kN corresponding to an axial strain of 0.02. Beyond that, the axial load dropped to 700 kN with a loss of approximately

60% at an axial strain of 0.027. This drop occurred due to rupture of the unidirectional FRP while the ±45° GFRP layers did not. After that, the axial load remained constant until an axial strain of 0.045. After that, the specimen displayed load softening until the failure of the specimen by the rupture of the ±45 GFRP layers at an axial strain of 0.11 (Fig. 9). The steel tube buckled locally as with the other specimens.

4.1.4. Group D (one layer of ±45° GFRP/two layers of unidirectional GFRP)

For specimen HC-GI45/II0-25-64, the load linearly increased until an axial load of 1720 kN corresponding to an axial strain of approximately 0.33% (Fig. 8d). Beyond that, the specimen displayed load hardening until the axial load reached its peak value of 2285 kN at an axial strain of 1.5%. Beyond the peak load, the axial load dropped to 670 kN with a loss of approximately 70% at an axial strain of 0.021 due to rupture of the unidirectional FRP, while the ±45° FRP did not suffer any rupture. Beyond that, the axial load softened until the ultimate axial strain of 0.11 when the specimen failed due to rupture of the ±45° FRP layers (Fig. 9). The steel tube buckled locally, which also occurred in the other specimens.

4.2. Discussions

4.2.1. Axial–hoop strains relation

Fig. 10 illustrates the hysteretic axial and hoop strains versus the axial load of each specimen. In this figure, the compressive strains are denoted with negative signs and vice versa.

The behaviors of the axial and hoop strains for the specimens in Groups A, B, and C were similar (Fig. 10a–c). In general, the axial and hoop strains of each specimen in these three groups increased simultaneously. The absolute values of the axial and hoop strains were close because of the ±45° fiber orientation.

During the first cycles, before the ultimate load, the hoop and axial strains increased linearly. At this stage, the concrete expansion under axial loading mainly occurred outwardly. At the ultimate load, the failure mainly occurred when the concrete lateral dilation broke the structure of the ±45° fibers and the epoxy. After this stage the fiber reorientation occurred and the specimen could not achieve higher strength. However, the axial and hoop strains did not reach to very high strains. This behavior occurred due to the steel tube's local buckling. When the steel tube buckled locally, the concrete expanded inwardly and outwardly. This behavior released some pressure on the FRP tube.

Three out of four specimens in Group B failed by FRP rupture, while none of the specimens in Group A failed by FRP rupture. This behavior was because the FRP tubes of the specimens in Group A were made out of carbon fibers, where the single carbon fiber had a lower diameter than the single glass fiber. Hence, the carbon fiber had a lower outer surface area compared to the glass fiber resulting in better epoxy impregnation in the glass fiber compared to the carbon fiber [24]. Therefore, the bond breakage of the structure of the ±45° fibers and the epoxy occurred earlier in the carbon fiber compared to the glass fiber. Once breakage occurred, the carbon fibers reoriented more than the glass fibers. This behavior caused the axial capacity of the specimens in Group A to be lower than those in Group B.

For specimen HC-GI45/II0-25-64 (Fig. 10d), at a given axial load, the value of the hoop strain was higher than the corresponding axial strain. This behavior indicated that the two unidirectional outer FRP layers reduced the reorientation of the ±45° fiber.

4.2.2. Change in FRP confinement

Fig. 11 shows the envelope of axial strains versus the normalized axial load for the specimens that had similar steel tubes and concrete shell thickness but different FRP confinement. There are discrepancies among different international codes when it comes to concrete filled tubes. The American Institute of Steel Construction (AISC) [25] used plastic-stress distribution method to calculate the equivalent uniform concrete stress while the ACI-318 [26] used Whitney stress block method. The plastic-stress distribution

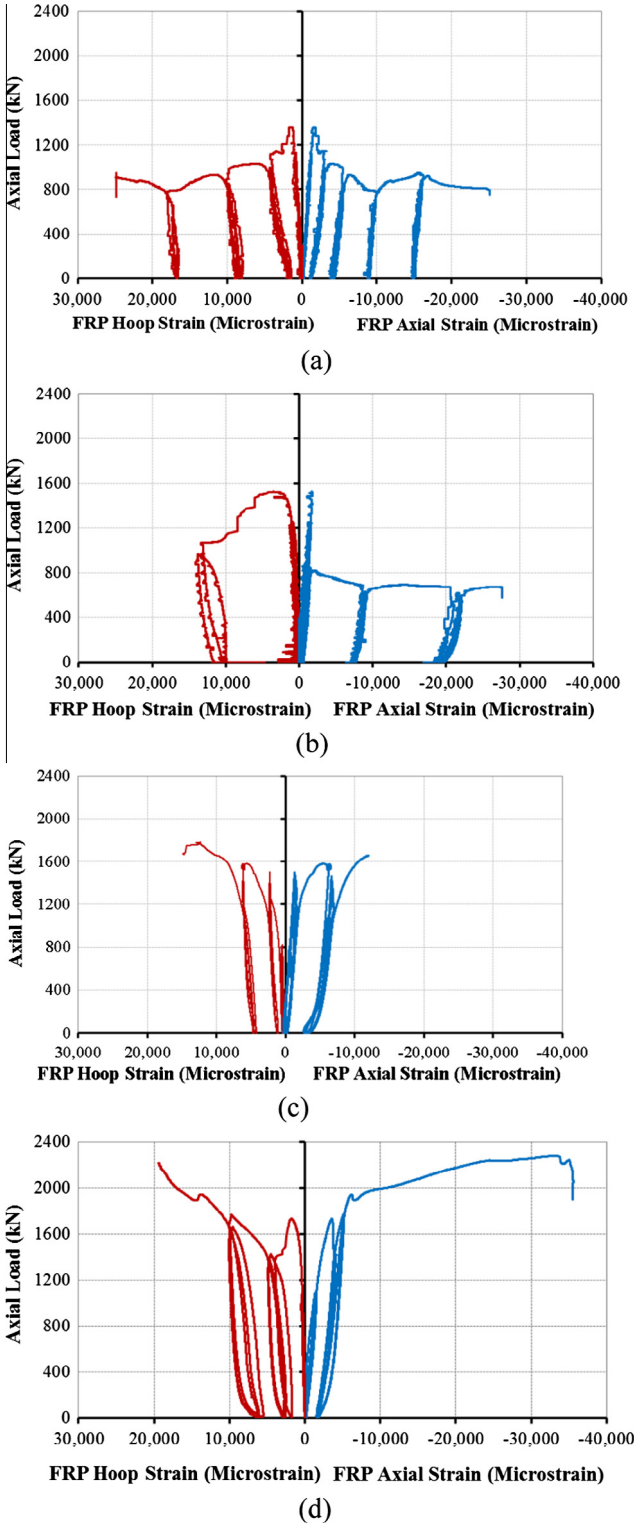

Fig. 10. FRP hoop strain and axial strain versus axial load relations of the specimens: (a) HC-CIII45-25-64, (b) HC-GIII45-25-64, (c) HC-GII45/I0-25-64, and (d) HC-GI45/II0-25-64.

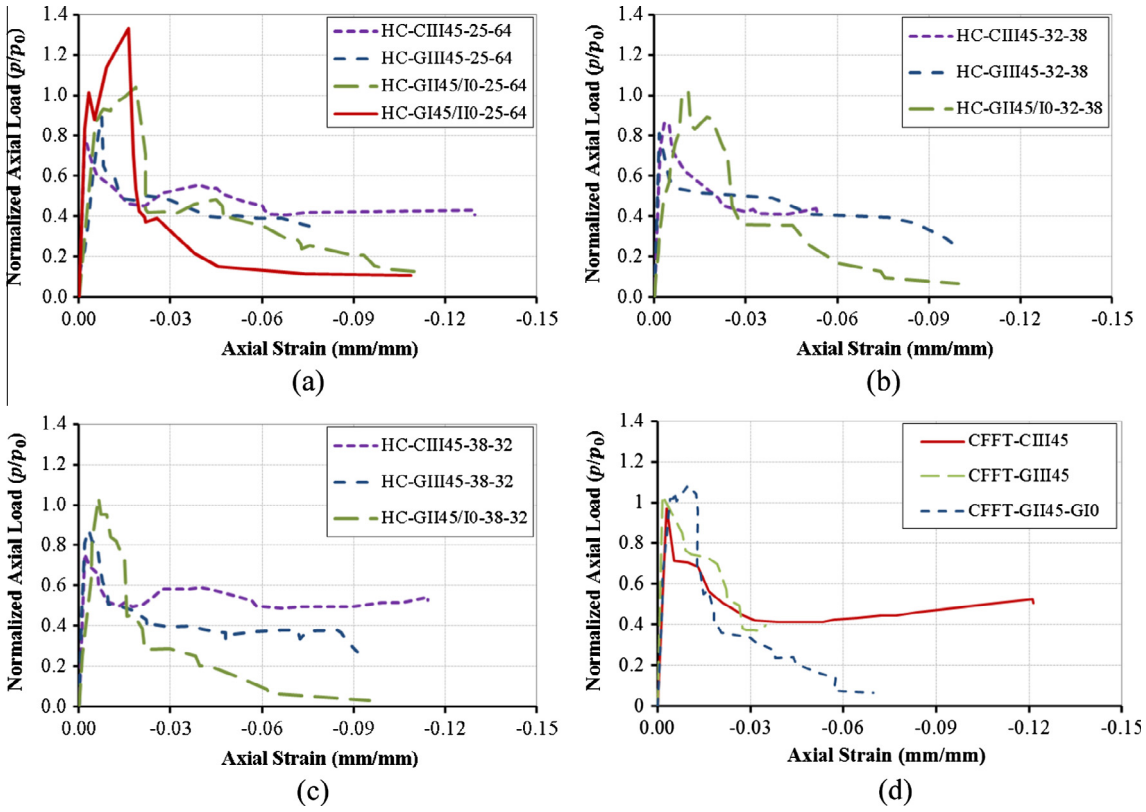

Fig. 11. Axial strain–normalized load relation of: (a) HCs with steel tube D/t ratio of 64, (b) HCs with steel tube D/t of 38, (c) HCs with steel tube D/t of 32, and (d) CFFTs.

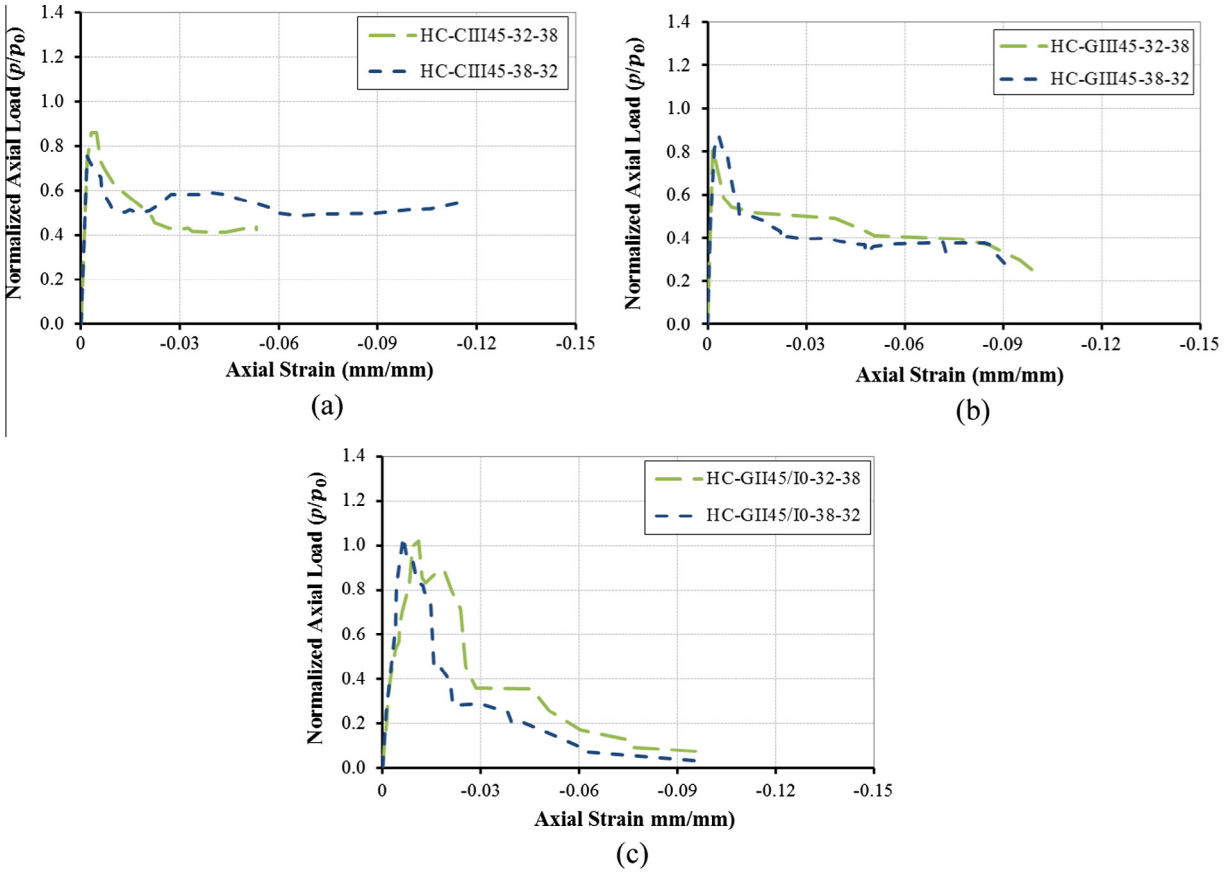

Fig. 12. Axial strain–normalized load relations of the two specimens of concrete shell thicknesses of 32% and 38% of: (a) Group A, (b) Group B, and (c) Group C.

Table 4
Steel tube D_i/t_s ratio of HC-FCS columns of literature and of current study.

	D_o (mm)	D_i (mm)	t_s (mm)	D_i/t_s	$(D_i/t_s)_{AISC}$	Normalized (D_i/t_s)	P_u/P_o
Current study	210	101.6	1.6	64.0	23.3	2.74	0.80
		101.6	1.6	64.0	23.3	2.74	0.89
		101.6	1.6	64.0	23.3	2.74	1.04
		101.6	1.6	64.0	23.3	2.74	1.30
		76.2	2.0	39.0	23.3	1.67	0.86
		76.2	2.0	39.0	23.3	1.67	0.82
		76.2	2.0	39.0	23.3	1.67	1.02
		50.8	1.6	32.0	23.3	1.37	0.76
		50.8	1.6	32.0	23.3	1.37	0.87
		50.8	1.6	32.0	23.3	1.37	1.04
Ozbakkaloglu and Fanggi [27]	150	101.6	3.2	31.8	35.0	0.91	1.31
		101.6	3.2	31.8	35.0	0.91	2.07
		101.6	3.2	31.8	35.0	0.91	1.05
		76.2	3.2	23.8	35.0	0.68	1.16
		76.2	3.2	23.8	35.0	0.68	1.17
		38.1	3.2	11.9	35.0	0.34	1.10
		38.1	1.6	23.8	35.0	0.68	1.27
		38.1	1.6	23.8	35.0	0.68	1.16
Yu et al. [13]	205	140.2	5.3	26.5	42.1	0.63	1.26
						0.63	1.23
Yu et al. [12]	152	76.2	3.2	23.8	41.1	0.58	0.99
						0.58	1.27
						0.58	1.48
Wong et al. [14]	152	41.9	2.3	18.3	38.7	0.47	1.35
		75.9	3.3	23.0	41.1	0.56	0.99
		75.9	3.5	21.7	34.2	0.63	1.14
		87.9	2.1	41.9	43.3	0.97	1.10
		115.1	5.2	22.1	39.5	0.56	1.17

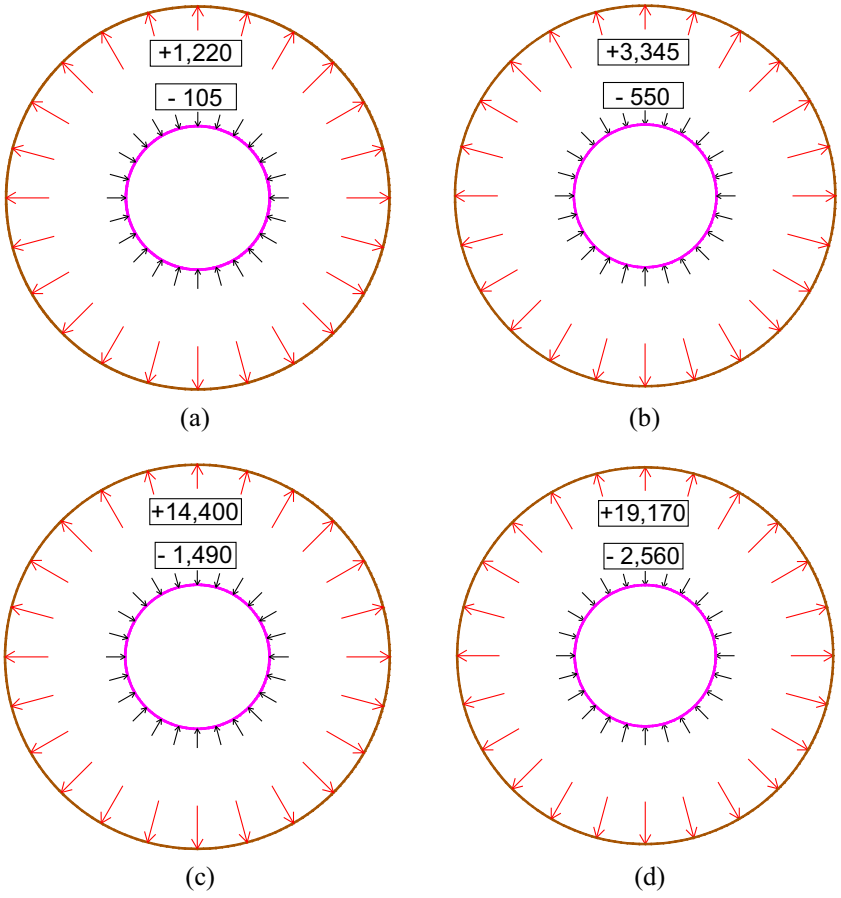

Fig. 13. FRP and steel hoop strains in the cross-sections of the specimens: (a) HC-CIII45-25-64, (b) HC-GIII45-25-64, (c) HC-GII45/I0-25-64, and (d) HC-GI45/II0-25-64.

revealed a concrete stress of 0.95 f'_c instead of 0.85 f'_c that is used by the ACI-318. The normalized axial load was calculated as the axial load over the nominal axial capacity (P_o) for a given specimen where P_o was calculated according to ACI-318 (Eq. (1)).

$$P_o = A_s f_y + 0.85 f'_c (A_c - A_s) \quad (1)$$

where A_s = the cross-sectional area of the steel tube, A_c = the cross-sectional area of the concrete shell, A_y = the yield stress of the steel tube, and f'_c = the cylindrical concrete's unconfined compressive stress.

Fig. 11a illustrates the relation of the axial strain versus the normalized axial load for the specimens that had a concrete shell thickness of 25% of the outer diameter. The normalized axial load increased from approximately 0.8 to 1.3 when the FRP tube structure was changed from one layer of ±45°/two layers of unidirectional to three layers of carbon fiber oriented at ±45°. The normalized axial load increased from approximately 0.8 to 1.04 when the FRP tube structure was changed from two layers of ±45°/one layer of unidirectional to three layers of carbon fiber oriented at ±45°.

Fig. 11b illustrates the relation of the axial strain versus the normalized axial load for the specimens that had a concrete shell thickness of 32% of the outer diameter. The normalized axial load increased from approximately 0.86 to 1.02 when the FRP tube structure was changed from two layers of ±45°/one layer of unidirectional carbon fibers to three layers of carbon fiber oriented at ±45°. However, the ultimate axial strains changed slightly.

Fig. 11c illustrates the relation of the axial strain versus the normalized axial load for the specimens that had a concrete shell thickness of 38% of the outer diameter. The normalized axial load increased from approximately 0.76 to 1.04 when the FRP tube structure was changed from two layers of ±45°/one layer of unidirectional carbon fibers to three layers of carbon fiber oriented at ±45°. However, the ultimate axial strains changed slightly.

Fig. 11d illustrates the relation of the axial strain versus the normalized axial load for the CFFT specimens. The normalized axial load increased from approximately 0.97 to 1.06 when the FRP tube structure was changed from two layers of ±45°/one layer of unidirectional carbon fibers to three layers of carbon fiber oriented at ±45°. The ultimate axial strains significantly changed (from 0.035 to 0.12) with the changing FRP type.

These comparisons indicated that increasing the FRP confinement improved the axial compressive strength of the HC-FCS specimens more than that of the CFFT specimens. However, the FRP confinement slightly affected the ultimate strains of the HC-FCS specimens, but it significantly affected the ultimate strains of the CFFT specimens.

4.2.3. Change in concrete shell thickness

Fig. 12 illustrates the axial strain versus the normalized axial load of the specimens that had concrete shell thicknesses of 32% and 38% of the outer diameter for all of the groups. These two specimens were selected from each group to investigate the effect of the concrete shell thickness on the axial capacity of the HC-FCS specimens. These specimens had close D_i/t_s ratios of steel tubes. Hence, the effect of the steel tube D_i/t_s ratio could be excluded from these comparisons. It should be noted that it was not possible to find steel tubes with different diameters but the same D_i/t_s in the local steel market. Fig. 12 shows that changing the concrete shell thickness had a negligible effect on the normalized axial capacity of the HC-FCS specimens if the steel tube D_i/t_s ratio was slightly changed.

4.2.4. Sectional analysis and steel tube local buckling

Using a D_i/t_s ratio is an important parameter in the study of HC-FCS columns. Previous studies were conducted on HC-FCS columns having low D_i/t_s values [12–14,27]. Table 4 summarizes the results of some previous studies on the HC-FCS columns under axial compressive loading. As shown in the table, the collected data is for stubs having D_i/t_s values ranging from 11.9 to 32 and P_u/P_o values ranging from 0.99 to 2.07. In the current study, specimens having D_i/t_s values ranged from 32 to 64 and P_u/P_o values ranged from 0.76 to 1.30. This low P_u/P_o is due to the reorientation of the fiber in the FRP tube and local buckling effects.

Fig. 13 illustrates, as an example, the hoop strains in the FRP and steel at a cross-section located at the mid-height of the specimens HC-CIII45-25-64, HC-GIII45-25-64, HC-GII45/I0-25-64, and HC-GI45/II0-25-64. These specimens had identical steel tubes while different FRP stiffness. The positive strain values represent tensile strain and vice versa. The reported strains corresponded to the peak load of each specimen. As shown in the figure, all of the steel tubes were subjected to compressive hoop strains while the FRP tubes were subjected to tensile hoop strains due to concrete dilation. The specimens HC-CIII45-25-64 and HC-GI45/II0-25-64 had the lowest and highest lateral pressure (i.e., lateral strain), respectively. As shown in the figure, there is a relation between the FRP confinement stiffness and the concrete lateral pressure. When the FRP confinement stiffness was increased, the concrete shell was laterally restrained from outside. Hence, the concrete dilation due to the axial compression directed toward the inner side, the weaker side, resulting in higher hoop compressive strains in the steel tube. The steel tube local buckling occurred due to the bidirectional compressive stress resulting from axial loads and concrete dilation. The hoop compressive strain in the steel tube of the specimen HC-GI45/II0-25-64 was approximately 2560 microstrain which is much higher than 105 microstrain in

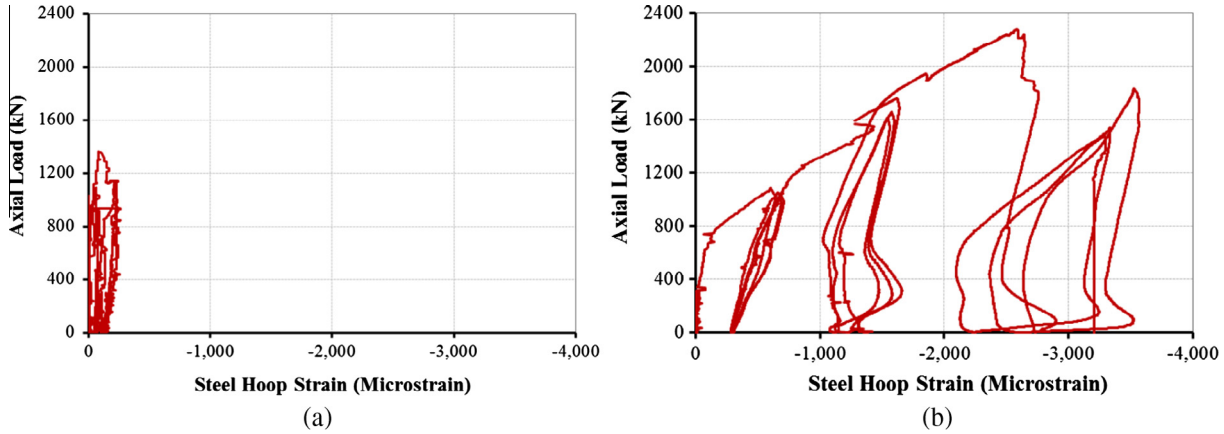

Fig. 14. Steel hoop strain–axial load relation of the specimens: (a) HC-CIII45-25-64 and (b) HC-GI45/II0-25-64.

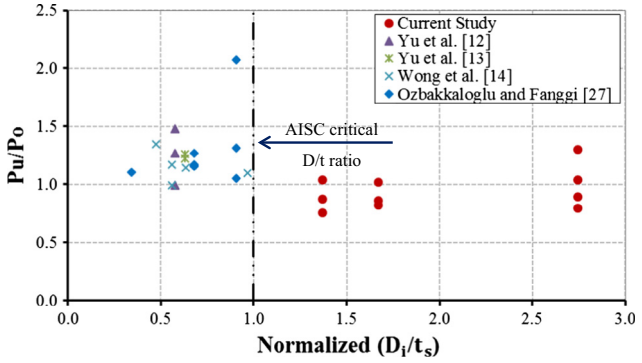

Fig. 15. Actual steel diameter–thickness ratios relative to the AISC manual value versus increase in capacity.

the case of the specimen HC-CIII45-25-64. Therefore, the steel tube was more susceptible to local buckling when the FRP confinement stiffness increased. Consequently, the specimen reached to higher axial strength and lower axial ductility when the FRP confinement stiffness increased. This indicated that the behavior of the HC-FCS columns under axial load is complicated, and it is related to the interaction between the FRP and steel stiffness. Further studies should be conducted to identify the relative steel–FRP tubes' stiffness for the optimum design.

Fig. 14 illustrates the hoop strains on the steel tubes of the specimens HC-CIII45-25-64 and HC-GI45/II0-25-64. As shown in Fig. 14b, the steel tube experienced local buckling at a load of 1500 kN corresponding to 1300 microstrain. Beyond that, the hoop strains unloading–reloading significantly changed. The specimen experienced significant residual hoop strains during the unloading behavior, indicating nonlinear buckling of the steel tube.

The normalized D_i/t_s can be defined as the ratio between the D_i/t_s and the D_i/t_s of the American Institute of Steel Construction (AISC) *Manual Steel Construction* [28] for steel columns with hollow sections under compression as per the following equation:

$$Normalized\ (D_i/t_s) = D_i/t_s \Big/ \left(0.07\frac{E}{F_y}\right) \quad (2)$$

where E and F_y are the Young's modulus and the yield stress of the steel tube, respectively.

As shown in Table 4 and Fig. 15, the local buckling occurred when the D_i/t_s ratio was higher than the AISC Manual value. The normalized D_i/t_s ratio for the tested cylinders in the current study was between 1.37 and 2.74. However, this ratio in the specimens gathered from the literature relative to the AISC manual was lower than 1.0, as shown in Fig. 15. That explained the local buckling that occurred for the steel tubes of the tested specimens, even for the specimens with a steel tube D_i/t_s ratio of 32.

According to the presented study, using steel tube D_i/t_s ratio of 64 is recommended for the HC-FCS columns under axial compressive loading which is agreed with the recommendations presented by Abdelkarim et al. [29] for the HC-FCS columns under combined flexural and axial compressive loading. More efficiency in strength and ductility can be achieved for the HC-FCS columns using this D_i/t_s ratio besides the cost benefits.

5. Findings and summary

The behavior of the hollow fiber reinforced polymer–concrete–steel columns (HC-FCS) under cyclic axial compressive loading was studied. The HC-FCS columns consisted of a concrete shell sandwiched between an outer FRP tube and an inner steel tube. Ten HC-FCS cylinders with different steel tube D_i/t_s ratios, three concrete-filled fiber tubes (CFFTs), and three steel tubes alone were tested under static cyclic axial compressive loading. The effects of using steel tubes with different D_i/t_s ratios and the effect of the FRP tube's fiber orientation on the behavior of the HC-FCS columns under axial load were investigated. The behavior of the HC-FCS columns was complicated and related mainly to the stiffness of the FRP and steel tubes, which controlled the direction of the concrete dilation under axial load. HC-FCS columns with FRP tubes made with fibers oriented at ±45° showed a low axial compressive strength and a high ultimate strain. HC-FCS columns with wet lay-up FRP tubes that had ±45° and 0° (hybrid FRP) exhibited high axial strengths and strains. The failure of the HC-FCS columns with hybrid FRP tubes consisted of two stages. The first stage was the rupture of the unidirectional FRP (outer tube), and the second stage was the reorientation of the ±45° fibers exhibiting high axial strains.

Acknowledgements

This research was supported by the Missouri Department of Transportation (MoDOT) and Mid-American Transportation Center (MATC) with contributions from the National University Transportation Center (NUTC) at Missouri University of Science and Technology (Missouri S&T). However, any opinions, findings, conclusions, and recommendations presented in this paper are those of the authors and do not necessarily reflect the views of the sponsors.

References

[1] Hajjar J. Concrete-filled steel tube columns under earthquake loads. Struct Eng Mater 2000;2(1):72–82.
[2] Shin, Andrawes B. Experimental investigation of actively confined concrete using shape memory alloys. J Eng Struct 2010;32(3):656–64.
[3] Zhu Z, Ahmad I, Mirmiran A. Seismic performance of concrete-filled FRP tube columns for bridge substructure. J Bridge Eng 2006;11(3):359–70.
[4] Dawood H, ElGawady M, Hewes J. Behavior of segmental precast post-tensioned bridge piers under lateral loads. ASCE J Bridge Eng 2012;17 (5):735–46.
[5] ElGawady M, Sha'lan A. Seismic behavior of self-centering precast segmental bridge bents. J Bridge Eng 2011;16(3):328–39.
[6] ElGawady M, Booker A, Dawood H. Seismic behavior of posttensioned concrete-filled fiber tubes. J Compos Constr 2010;14(5):616–28.
[7] Montague P. Experimental behavior of double-skinned, composite, circular cylindrical shells under external-pressure. J Mech Eng Sci 1978;20(1):21–34.
[8] Shakir-Khalil H, Illouli S. Composite columns of concentric steel tubes. In: Proc., conf. on the design and construction of non-conventional structures, vol. 1, London; 1987. p. 73–2.
[9] Yagishita F, Kitoh H, Sugimoto M, Tanihira T, Sonoda K. Double-skin composite tubular columns subjected cyclic horizontal force and constant axial force. In: Proceedings of the sixth ASCCS conference, Los Angeles, USA; March 22–24, 2000. p. 497–03.
[10] Teng JG, Yu T, Wong YL. Behavior of hybrid FRP–concrete–steel double-skin tubular columns. In: Proc. 2nd int. conf. on FRP composites in civil engineering, Adelaide, Australia; 2004. p. 811–18.
[11] Li W, Han LH, Chan T. Tensile behaviour of concrete-filled double-skin steel tubular members. J Constr Steel Res 2014;99:35–46.
[12] Yu T, Wong YL, Teng JG, Dong SL. Structural behavior of hybrid FRP–concrete–steel double-skin tubular columns. In: ANCER annual meeting: networking of young earthquake engineering researchers and professionals, Honolulu, Hawaii; 2004.
[13] Yu T, Wong YL, Teng JG. Behavior of hybrid FRP–concrete–steel double-skin tubular columns subjected to eccentric compression. Adv Struct Eng 2010;13 (5):961–74.
[14] Wong YL, Yu T, Teng JG, Dong SL. Behavior of FRP-confined concrete in annular section columns. Compos: Part B Eng 2008;39:451–66.
[15] Teng JG, Yu T, Wong YL, Dong SL. Innovative FRP–steel–concrete hybrid columns. Adv Steel Struct 2005;1:545–54.
[16] Teng JG, Yu T, Wong YL, Dong SL. Hybrid FRP concrete-steel tubular columns: concept and behavior. Constr Build Mater 2007;21(4):846–54.
[17] Karbhari VM, Eckel DA, Tunis GC. Strengthening of concrete column stubs through resin infused composite wraps. J Therm Comp Mat 1993;6:92–106.
[18] Howie I, Karbhari VM. Effect of two sheet composite wrap architecture on strengthening of concrete due to confinement: I-experimental studies. J Reinf Plast Compos 1995;14:1008–30.
[19] Mirmiran A, Kargahi M, Samaan M, Shahawy M. Composite FRP–concrete column, with bi-directional external reinforcement. In: Fiber composites in

infrastructure: proc., 1st international conf. in composites in infrastructure ICCI'96; 1996.
[20] Picher F, Rochette P, Labossiere P. Confinement of concrete cylinders with CFRP. In: Fiber composites in infrastructure: proc., 1st international conf. on composites in infrastructure, Tuscon, Ariz; 1996. p. 829–41.
[21] Au C, Buyukozturk O. Effect of fiber orientation and ply mix on fiber reinforced polymer-confined concrete. J Compos Constr 2005;9(5):397–407.
[22] ASTM Standard D3039. Standard test method for tensile properties of polymer matrix composite materials. ASTM International, West Conshohocken, PA; 2008. http://dx.doi.org/10.1520/D3039_D3039M-08.
[23] ASTM Standard A1067. Test coupons for steel castings. ASTM International, West Conshohocken, PA; 2012. http://dx.doi.org/10.1520/A1067_A1067M-12A.
[24] Wang R-M, Zheng S-R, Zheng Y-P. 4 – Interface of polymer matrix composites. In: Wang R-M, Zheng S-R, Zheng Y-P, editors. Polymer matrix composites and technology. Woodhead Publishing; 2011. p. 169–548.
[25] AISC. "Specifications for structural steel buildings" ANSI/AISC standard 360-05. Chicago, IL: American Institute of Steel Construction; 2005.
[26] ACI Committee 318. Building code requirements for structural concrete (ACI318-14) and commentary (318R-14). Farmington Hills, Mich: American Concrete Institute; 2014, 509 pp.
[27] Ozbakkaloglu T, Fanggi B. Axial compressive behavior of FRP–concrete–steel double-skin tubular columns made of normal- and high-strength concrete. J Compos Constr 2013. http://dx.doi.org/10.1061/(ASCE)CC.1943-5614.0000401, 04013027.
[28] AISC. Manual of steel construction. 14th ed. Chicago: American Institute of Steel Construction; 2011. 2011.
[29] Abdelkarim O, Gheni A, Anumolu S, Wang S, ElGawady M. Hollow-core FRP–concrete–steel bridge columns under extreme loading. Missouri Department of Transportation (MoDOT), Project No. TR201408, Report No. cmr15-008; 2015 April.